Electron mobility estimation of hollow cathode plasma in different electrical configurations

IEPC-2025-455

Presented at the 39th International Electric Propulsion Conference
Imperial College London, London, UK
September 14-19, 2025

Yusuke Yamashita[1],
Stanford University, Stanford, California 94305, USA

Naia Butler-Craig[2], Mitchell L. R. Walker[3]
Georgia Institute of Technology, Atlanta, Georgia 30332, USA

Kentaro Hara[4]
Stanford University, Stanford, California 94305, USA

In Hall effect thrusters (HETs), several experimental works suggest that the thruster performance (e.g., discharge current oscillation) is affected by the electrical configurations of the thruster body. Recent measurement data of the electron density n_e and electron temperature T_e obtained from the incoherent laser Thomson scattering show that the near-field hollow cathode discharge is also affected depending on the electrical configuration in a center-mounted HET. In this study, the measurement data of n_e and T_e are input to a one-dimensional fluid model, and the electron mobility is estimated for three electrical configurations: ground, floating, and cathode-tied. The estimated results, such as the anomalous electron scattering frequency, agree with the literature. In addition, the estimated results suggest that the electron mobility is the highest for the ground condition, while the electron conductivity is comparable between the floating and cathode-tied conditions.

I. Introduction

Electric propulsion (EP) devices have been tested in ground facilities (i.e., a vacuum chamber) for predicting thruster performance (e.g., thrust and lifetime). However, several in-space operations have clarified the difference in thruster performance between ground tests and space operations[1–4], which is attributed to the so-called facility effect. Facility effects are mainly divided into three problems [5]: background pressure, contamination, and electrical facility effects.

In this paper, we focus on the electrically facility effect in Hall effect thrusters (HETs). Figure 1 shows three electrical configurations of the thruster body in HET. For the ground configuration, the thruster body is connected to the chamber ground. For the floating configuration, the thruster is electrically isolated from the chamber ground. Finally, for the cathode-tied configuration, the thruster voltage is equal to the cathode voltage relative to the ground, $V_{c,g}$. Several works suggest that thrust [6], the discharge current [6–8], and the discharge current oscillations [6, 8–10] are affected by the electrical configurations. In addition, a recent study shows the electron properties (e.g., electron density and temperature) at near-field hollow cathode discharge are also modified by the electrical configuration, as measured by incoherent laser Thomson scattering (LTS) [10]. In this work, the experimental data of the electron density and temperature is input into a one-dimensional fluid model, and then the electrical mobility is estimated in different electrical configurations.

[1]Postdoctoral Researcher, Aeronautics and Astronautics, yamashita.yusuke@jaxa.jp
[2]Graduate Research Assistant, School of Aerospace Engineering, naiabc3@gatech.edu
[3]Professor, School of Aerospace Engineering, mitchell.walker@ae.gatech.edu
[4]Assistant Professor, Aeronautics and Astronautics, kenhara@stanford.edu

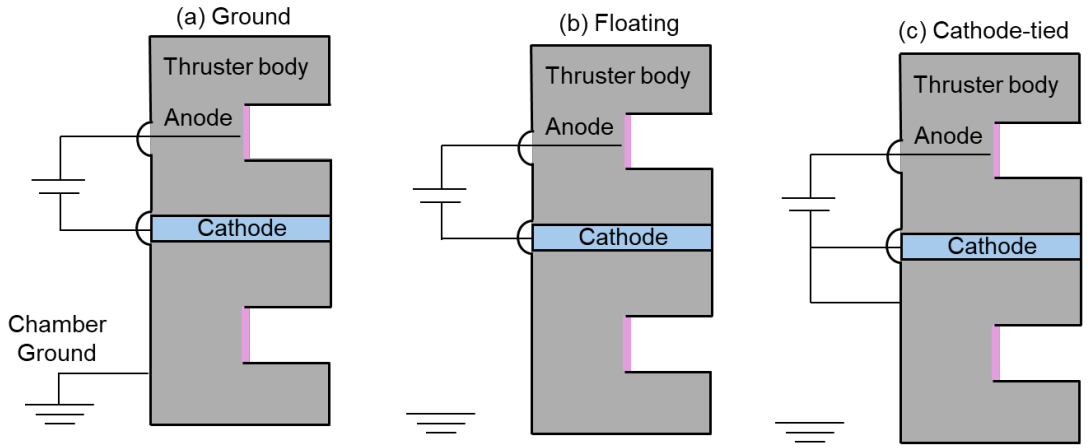

Fig. 1 Electrical configuration of the thruster body in HET. The testing was performed with three different electrical configurations: (a) ground, (b) floating, and (c) cathode tied.

II. Experimental condition and data

In this paper, experimental data of the hollow cathode plume are used [10]. The H9 thruster is operated with an input power of 6 kW, where the discharge voltage is V_d = 300 V and the discharge current is I_d = 20 A, in the VTF-2 vacuum chamber at Georgia Institute of Technology. A hollow cathode is mounted at the center of the HET. The working gas is krypton, and the mass flow at the cathode $\dot{m}_c$ is 1.26 mg/s. Figure 2 shows (a) n_e and (b) T_e for three electrical configurations. Symbols show the experimental data of n_e and T_e obtained from the LTS measurement. In this study, to substitute the experimental data into a one-dimensional fluid model, polynomial fitting is performed. In addition, the experimental uncertainty is assumed to be 15% for both n_e and T_e. That is, each data point is generated considering the experimental uncertainty using a random number, and then polynomial fitting is performed. By repeating this procedure many times (e.g., 10^4), the mean value and standard deviation σ are evaluated for n_e and T_e. In Fig. 2, the solid line shows the mean value, and the shadow region shows 2σ, respectively.

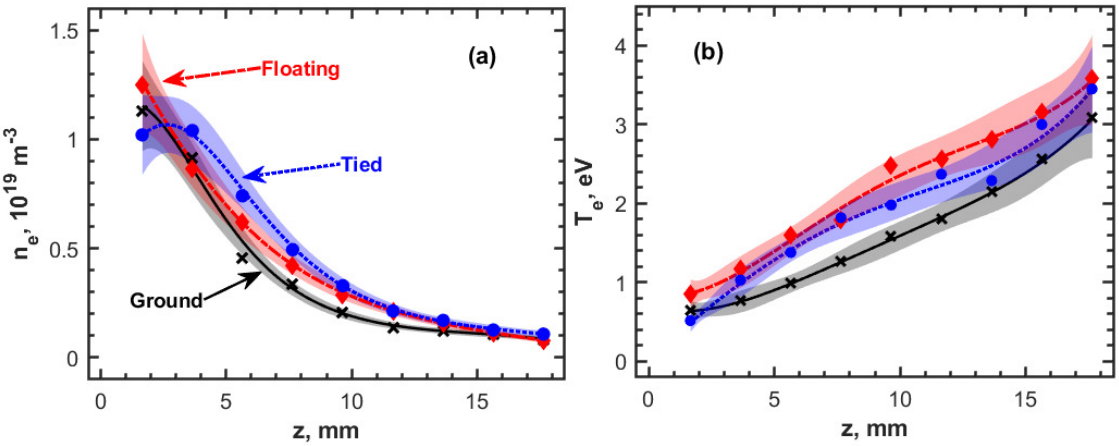

Fig. 2 (a). n_e, (b) T_e in three electrical configurations: ground, floating, and tied. Symbol: experimental data obtained from the incoherent laser Thomson scattering [10]. Solid line: mean value of the polynomial fitting. Shadow region: 2σ of the polynomial fitting. In this study, $\pm$15% uncertainty of experimental data is considered.

III. Estimation of electron mobility

The effective electron mobility μ_{eff} is defined as,

$$n_e u_{e,z} = -\mu_{\text{eff}} \left(n_e E_z + \frac{1}{e} \frac{\partial p_e}{\partial z} \right). \tag{1}$$

where n_e is electron density, $u_{e,z}$ is axial electron bulk velocity, E_z is axial electric field, e is elementary charge, and $p_e = n_e k_B T_e$ is electron pressure (k_B: Boltzmann constant and T_e is electron temperature). μ_{eff} is defined as,

$$\mu_{\text{eff}} = \frac{e}{m_e(\nu_m + \nu_{\text{ano}})}, \tag{2}$$

where ν_m is the momentum transfer collision frequency, and ν_{ano} is anomalous scattering frequency. Since LTS measurements provide n_e and T_e, E_z and $u_{e,z}$ are estimated using quasi-1D, steady-state, fluid models. Here, we use the neutral continuity, ion continuity, ion momentum equations, and current conservation [11].

$$u_{n,z} \frac{dn_n}{dz} = -k_{iz} n_e n_n - \frac{u_{n,r}}{\Delta R} n_n, \tag{3}$$

$$\frac{d(n_i u_{i,z})}{dz} = k_{iz} n_e n_n - \frac{u_{i,r}}{\Delta R} n_n. \tag{4}$$

$$m_i \frac{d(n_i u_{i,z}^2)}{dz} + eT_i \frac{dn_i}{dz} = en_i E_z + m_i k_{iz} n_e n_n u_{n,z} - m_i \frac{u_{i,r}}{\Delta R} n_i u_{i,z}. \tag{5}$$

$$I_d = en_i(u_{i,z} - u_{e,z})A. \tag{6}$$

where n_n is neutral density, $u_{n,z}$ and $u_{n,r}$ are axial and radial neutral velocities which assume a constant thermal velocity, k_{iz} is the rate coefficient of ionization which is function of T_e if assuming Maxwellian distribution, n_i is ion density which assumes quasi-neutral ($n_i \approx n_e$), $u_{i,z}$ and $u_{i,r}$ are axial and radial ion velocities, ΔR is the characteristics length of ambipolar type diffusion, I_d is the discharge current, $u_{e,z}$ is axial ion velocity, and A is the surface area.

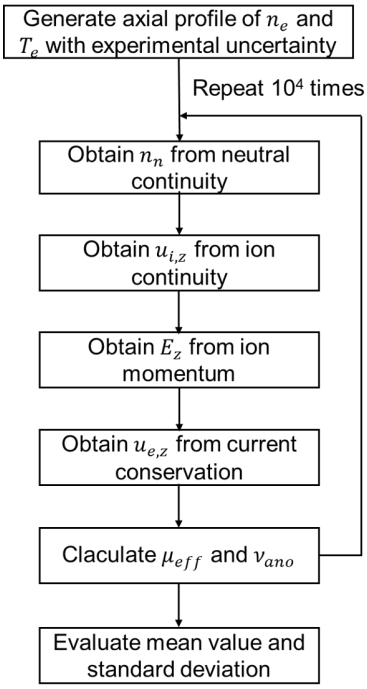

Fig. 3 Flow chart for estimation of electron mobility from the experimental data of n_e and T_e. Uncertainty quantification is performed considering the uncertainty of experimental data and assumptions.

Figure 3 shows the flow chart for the estimation of μ_{eff} and ν_{ano}. In this case, since n_e and T_e are provided from the experiment, data assimilation techniques, such as Kalman filters [12], are not required. First, n_n is estimated from Eq.(3). Second, $u_{i,z}$ is estimated from Eq.(4). Third, E_z is estimated from Eq.(5). Fourth, $u_{e,z}$ is estimated from Eq.(6). Then, μ_{eff} and ν_{ano} are obtained from Eqs. (1) and (2). It should be noted that $n_n(z=0) = 0.8\dot{m}_c/(Au_{n,z})$ is used when solving Eq.(3), and the ion bulk velocity at the plume is specified when solving when solving Eq. (4).

Uncertainty quantification is performed to evaluate the experimental uncertainty and the assumed uncertainty. In this study, the experimental uncertainty is assumed to be 15% for both n_e and T_e. In addition, for the assumed uncertainty, $T_n = 500 - 1500$ K, $u_{i,z_p} = 2000 - 3000$ m/s, $T_i = 0.1 - 1.0$ eV are used. Each parameter is generated randomly between the range shown above, and then the mean value and standard deviation of μ_{eff} and ν_{ano} are estimated.

IV. Estimated results

Figure 4 shows the estimated μ_{eff} and classical mobility ν_{ano} in three electrical configurations using three values of $\Delta R = 5,\ 6,\ 7$ mm. For (a1). $\Delta R = 5$ mm, it can be seen that μ_{eff} is the order of $10^2 - 10^3$ $\text{m}^2\text{V}^{-1}\text{s}^{-1}$ and μ_{eff} is one or two orders of magnitude smaller than the classical mobility, indicating the presence of the anomalous collision frequency. Figure 4 (a2) indicates that ν_{ano} is the order of $10^8 - 10^9$ Hz, which is in good agreement with the literature [13–16]. Figures 4(a1), (b1), and (c1) suggest that μ_{eff} is not changed too much for different ΔR. Both $|E_z|$ and $u_{e,z}$ become small when using large ΔR, and thus μ_{eff} is not much sensitive to ΔR from Eq. (1). It should be noted that there is a large uncertainty around $z = 1.75$ mm. In some cases, $|E_{\text{eff}}| = E_z + (en_e)^{-1}\partial p_e/\partial z$ is close to 0 and μ_{eff} becomes large significantly, resulting in the large uncertainty. The improvement of the boundary condition around $z = 1.75$ mm is reserved for future work.

Most interestingly, μ_{eff} (i.e., electron conductivity) is the largest for the ground condition, while μ_{eff} of the floating condition is comparable to the tied condition. Interpolation of μ_{eff} for three electrical configurations is reserved for future work.

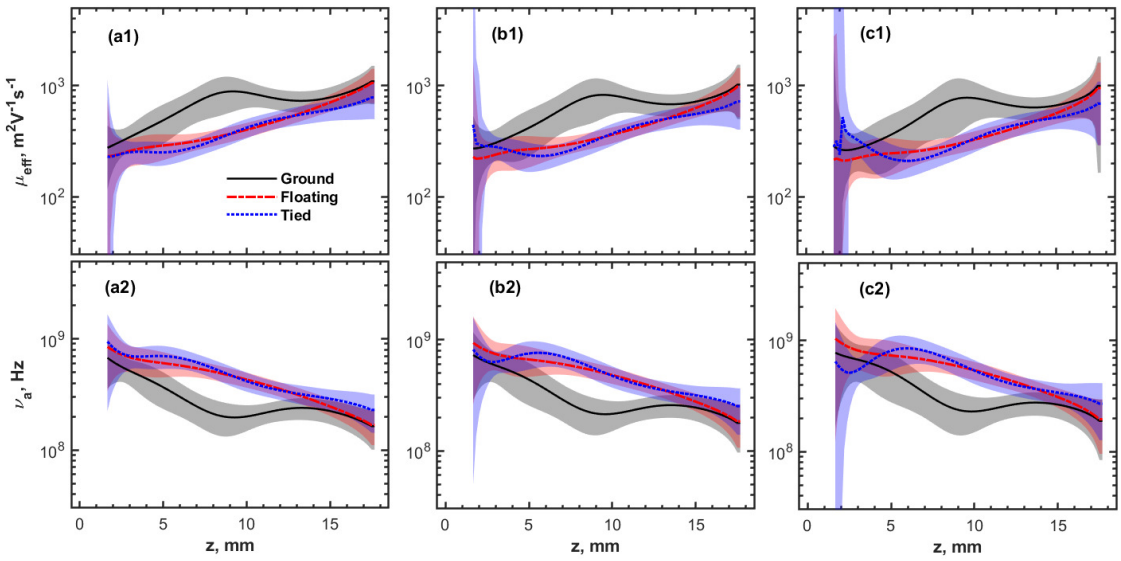

Fig. 4 Estimated properties: (1). μ_{eff} and (2). ν_{ano} for three electrical configurations: ground, floating, and tied. Solid line: mean value, shadow regions: 2σ including the uncertainty of the experimental data shown in Fig. 2 and the assumed uncertainty. (a). $\Delta R = 5$ mm, (b). $\Delta R = 6$ mm, and (c). $\Delta R = 7$ mm.

V. Conclusion

In this paper, the electron mobility is estimated at a near-field hollow cathode discharge using a 1D fluid model based on measurement data of electron density and electron temperature obtained from incoherent laser Thomson scattering. The estimation is performed for three electrical configurations of the thruster body: ground, floating, and cathode-tied. The estimated results suggest that the electron conductivity is the highest for the ground configuration,

while the electron conductivity is comparable between the floating and cathode-tied conditions.

Acknowledgments

This work was supported by NASA through the Joint Advanced Propulsion Institute, a NASA Space Technology Research Institute under Grant No. 80NSSC21K1118.

References

[1] Manzella, D., Jankovsky, R., Elliott, F., Mikellides, I., Jongeward, G., and Allen, D., "Hall thruster plume measurements on-board the Russian express satellites," *27th International Electric Propulsion Conference*, 2001.

[2] Passaro, A., Vicini, A., Nania, F., and Biagioni, L., "Numerical Rebuilding of SMART-1 Hall effect thruster plasma plume," *Journal of Propulsion and Power*, Vol. 26, No. 1, 2010, pp. 149–158.

[3] Nishiyama, K., Hosoda, S., Tsukizaki, R., and Kuninaka, H., "In-flight operation of the Hayabusa2 ion engine system on its way to rendezvous with asteroid 162173 Ryugu," *Acta Astronautica*, Vol. 166, 2020, pp. 69–77.

[4] Polk, J., Kakuda, R., Anderson, J., Brophy, J., Rawlin, V., Sovey, J., and Hamley, J., "In-flight performance of the NSTAR ion propulsion system on the Deep Space One mission," *2000 IEEE Aerospace Conference. Proceedings (Cat. No. 00TH8484)*, Vol. 4, IEEE, 2000, pp. 123–148.

[5] Foster, J. E., and Topham, T. J., "A review of the impact of ground test-related facility effects on gridded ion thruster operation and performance," *Physics of Plasmas*, Vol. 31, No. 3, 2024.

[6] Peterson, P. Y., Kamhawi, H., Huang, W., Williams, G., Gilland, J. H., Yim, J., Hofer, R. R., and Herman, D. A., "Nasa's Hermes hall thruster electrical configuration characterization," *52nd AIAA/SAE/ASEE Joint Propulsion Conference*, 2016, p. 5027.

[7] Frieman, J. D., Walker, J. A., Walker, M. L., Khayms, V., and King, D. Q., "Electrical facility effects on Hall thruster cathode coupling: Performance and plume properties," *Journal of Propulsion and Power*, Vol. 32, No. 1, 2016, pp. 251–264.

[8] Jovel, D. R., Cabrera, J. D., and Walker, M. L., "Current pathways model for hall thruster plumes in ground-based vacuum test facilities: measurements and observations," *Journal of Electric Propulsion*, Vol. 3, No. 1, 2024, p. 35.

[9] Walker, J. A., Frieman, J. D., Walker, M. L., Khayms, V., King, D., and Peterson, P. Y., "Electrical facility effects on Hall-effect-thruster cathode coupling: Discharge oscillations and facility coupling," *Journal of Propulsion and Power*, Vol. 32, No. 4, 2016, pp. 844–855.

[10] Butler-Craig, N. I., Suazo Betancourt, J. L., Lopez-Uricoechea, J., Lev, D., and Walker, M. L., "Comparison of the Near-Field Electron Properties of the H9 Hall Effect Thruster in Various Electrical Configurations With Incoherent Laser Thomson Scattering," *AIAA SCITECH 2025 Forum*, 2025, p. 1099.

[11] Hara, K., and Mikellides, I. G., "Characterization of low frequency ionization oscillations in Hall thrusters using a one-dimensional fluid model," *2018 Joint Propulsion Conference*, 2018, p. 4904.

[12] Dwivedi, A., Cerepi, M., and Hara, K., "Spatiotemporal state and parameter estimation of plasma dynamics using data assimilation," *Physics of Plasmas*, Vol. 32, No. 6, 2025.

[13] Georgin, M. P., Jorns, B. A., and Gallimore, A. D., "Transient non-classical transport in the hollow cathode plume I: measurements of time-varying electron collision frequency," *Plasma Sources Science and Technology*, Vol. 29, No. 10, 2020, p. 105010.

[14] Georgin, M. P., and Jorns, B. A., "Transient non-classical transport in the hollow cathode plume II: evaluation of models for the anomalous collision frequency," *Plasma Sources Science and Technology*, Vol. 29, No. 10, 2020, p. 105011.

[15] Georgin, M. P., and McDonald, M. S., "Experimental evaluation of the 2D non-classical ohmic transport model for electrons in the hollow cathode plume," *Journal of Applied Physics*, Vol. 130, No. 20, 2021.

[16] Ortega, A. L., Jorns, B. A., and Mikellides, I. G., "Hollow cathode simulations with a first-principles model of ion-acoustic anomalous resistivity," *Journal of Propulsion and Power*, Vol. 34, No. 4, 2018, pp. 1026–1038.